Meta-surface Boosted Antenna to achieve higher than 50 dB TRX Isolation at 26 GHz for Joint Communication and Radar Sensing (JC&S)

Mehrab Ramzan, Andre N. Barreto, and Padmanava Sen

Barkhausen Institut, Dresden, Germany
Email: {mehrab.ramzan, andre.nollbarreto, padmanava.sen,}@barkhauseninstitut.org

***Abstract*—In this paper, sub-wavelength passive periodic structures are used to create high isolation between the transmitter (Tx) and receiver (Rx) antennas designed at 26 GHz. The periodic electromagnetic bandgap (EBG) structures composed of square mushroom shapes are used between Tx and Rx (TRX) antennas for increasing the isolation from 22 dB to 50 dB experimentally. The results are compared in terms of simulation and measurement and a close agreement is found between them. Moreover, the results are further used to extract system performance targeting joint communication and radar sensing (JC&S) applications.**

I. Introduction

Sensing is widely seen as one of the key technologies in the sixth generation (6G) of wireless communication systems [1], allowing a plethora of new services and applications. It is envisaged that radar sensing, in particular, will be integrated with the communications network [2], such that it can be offered as an additional service upon demand, in what we call Radar as a Service (RaaS). Currently, radar and wireless communication systems are designed and deployed separately, using different hardware and waveforms, and distinct parts of the spectrum. A joint communication and radar sensing (JC&S) system will benefit the over-crowded communication space with spectrum sharing, by using part of the radar spectrum. Besides, the use of communication technologies will enable a coordinated systems of radars, currently struggling with increasing interference between different radars. Finally, connected radars may exchange information, allowing a better detection performance by means of sensor fusion, enabling many new services.

Antenna design plays a significant role in making such future systems a reality. Most automotive radar systems today use separate antennas for transmitting and receiving [3] , for example, in frequency-modulated continuous wave (FMCW) radars, whereas in upcoming communication systems there is a strong push towards full-duplex (FD) systems, in which transmitters and receivers can operate at the same time. A full-duplex radio, also known as simultaneous transmit and receive (STAR) capable radio, can thus increase the capacity of wireless networks through an efficient reuse of the allocated electromagnetic spectrum (EMS). For communications, the major advantage provided by STAR is to potentially double the spectral efficiency compared to widely used half-duplex radio links based on time or frequency division duplex [4], but accounting for traffic asymmetry and the increased interference, the capacity gains are usually less than that. For radar detection, on the other hand, STAR is essential, because the device must be able to transmit and detect the returning echos simultaneously.

In a STAR system, either one must integrate a circulator in the RF front-end or use two separate antennas with sufficient isolation. Currently available circulator topologies do not support reliably more than 20 dB transmitter-to-receiver isolation over the full operating band [4]. This limitation has been one of the bottlenecks of STAR-capable radios in communication systems and radars. In this work, we demonstrated higher-than-50 dB measured TRX antenna isolation using meta-surfaces, thus enabling a JC&S system with STAR capable communication and radars (e.g. FMCW radars).

The mutual coupling issues between the antennas are already comprehensively addressed in [5], [6]. There are numerous methodologies to mitigate this mutual coupling between the antennas using active circuitry [7]. However, active circuits do not only increase the complexity of the whole system, but they are also power-hungry, making them inefficient and difficult to implement for the future 6G JC&S applications in battery driven devices. According to the literature, electromagnetic bandgap (EBG) structures are already known but the achieved isolation with these structures is less than 30 dB [8]. In this paper, we discuss how these passive EBG meta-surfaces can be used at 5G NR cmWave bands (26 GHz) to achieve high isolation between the transmitting and receiving antennas. This approach not only saves power, but it is also a cost-effective method for future compact radar and communication systems.

In this work, existing 5G NR communication band with 400 MHz available bandwidth is chosen for proof-of-concept demonstration, as JC&S frequency bands are not yet decided. The coupling values of the antenna board without the passive electromagnetic bandgaps are simulated and used as a reference for the Tx and Rx board with the EBG, and compared in terms of isolation, bandwidth and gain pattern. The final board is fabricated and compared to the simulated results. Furthermore, the results are used to evaluate the JC&S radar

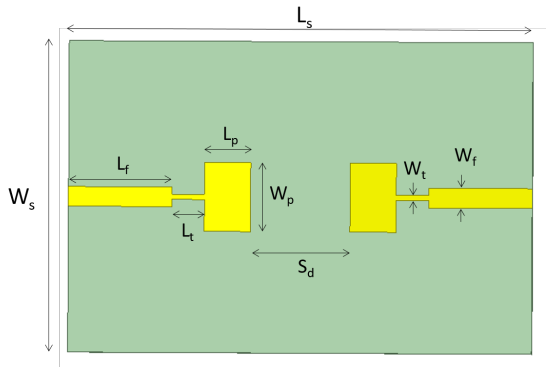

Fig. 1. Simulation model with highlighted dimensions of Tx and Rx antenna without EBG

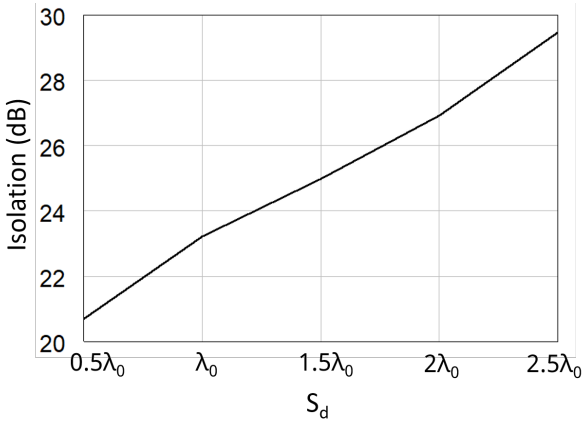

Fig. 2. Isolation between Tx and Rx antenna as a function of separation distance

performance, which can be severely affected by the self-interference component caused by low TRX isolation. The paper is organized as follows. In Section II the simulation results of achieving isolation without EBG structures are discussed, and in Section III the simulation and measured results of the transmitter and receiver antenna with EBG structures are analyzed. In section IV, the results are used to evaluate the system performance feasibility of the whole Tx and Rx board for the future JC&S applications. Finally, the conclusion and future work of the paper are presented in Section V.

II. Tx and Rx without EBG

The simplest way of achieving high isolation between the transmitter (Tx) and receiver (Rx) antennas is by increasing the separation distance S_d between the Tx and Rx antennas. This technique of increasing the isolation is shown by two microstrip patch antennas, one used as the transmitter antenna and the other as the receiver antenna, as shown in Fig. 1.

Fig.2 shows the isolation values with respect to the separation distance between the antennas S_d, which is changed from $0.5\lambda_0$ to $2.5\lambda_0$, with λ_0 the free space wavelength at 26 GHz. At $S_d = 0.5\lambda_0$ the isolation between the Tx and Rx antennas is around 21 dB and when the separation distance is increased to $2.5\lambda_0$, the isolation becomes around 29 dB. In order to achieve isolation higher than 30 dB, a distance of more than $3\lambda_0$ is required. Nevertheless, increasing the isolation between the Tx and Rx antennas requires a lot of board area and it is not an optimal solution for compact designs. Therefore, metamaterials can be one of the best contestants not only for increasing the isolation but also for keeping the distance between the Tx and Rx antennas fixed to a sub-wavelength value.

III. Tx and Rx antennas with EBG

In this section, the electromagnetic bandgap (EBG) structure and its integration between the transmitting and receiving antennas are discussed. Sub-wavelength periodic structures can be used for the creation of electromagnetic bandgaps. These periodic structures create a bandgap in the desired spectrum, in which the propagation of electromagnetic waves is restricted. This phenomenon of restricted propagation can be used to suppress the surface waves and, thus, to create a high isolation between the transmitter and receiver antennas for JC&S applications. The EBG structures are designed on the basis of mushroom-type structures, as shown in Fig. 3. The mushroom structure consists of a square patch at the top with a centred shortening via at the middle of the patch connecting it to the ground plane. The mushroom structure behaves like a resonator, where its inductance is controlled by the via and its capacitance is decided by the inter-spacing of the top square patches.

The Tx and Rx board with EBG is designed on a low cost RF substrate of rogers 4003C with a permittivity of 4.55 and tanδ of 0.0027. The thickness of the substrate is chosen to be 0.508 mm. The extracted EM bandgap diagrams [9] of the periodic mushroom structures are shown in Fig. 4. The optimized unit cell dimensions are given in Table I, which are chosen to have an EM bandgap in the regime of 26 GHz of the designed frequency. The design flow of the highly isolated transmitter and receiver antenna is shown in Fig. 5. In the initial step, the unit cell simulation is done using eigenmode solver of HFSS. In the next step, the electromagnetic bandgap diagrams from the different excited modes during the eigenmode simulations are extracted. In the final phase, the EBG structures are integrated between the transmitter and receiver antennas and the results are optimized for the designed frequency.

The simulation model of Tx and Rx board with EBG structures and highlighted dimensions is shown in Fig. 6. The distance between the Tx and Rx antennas is fixed to 0.75 λ_0 to incorporate enough unit cells of EBG and leave some extra space for not deteriorating the radiation pattern of the antenna. In order to have a good agreement between the measured and simulated results, the connector dimensions, shortening-via and copper-etching tolerance of the patches are carefully taken into account during the simulations. The optimized dimensions of the board are given in Table I. The comparison of the antenna performance parameters with and without EBG structures is provided in Table II. According to the simulation

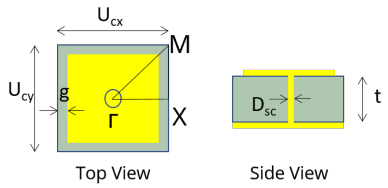

Fig. 3. Unit cell overview of the EBG for extracting electromagnetic band diagrams

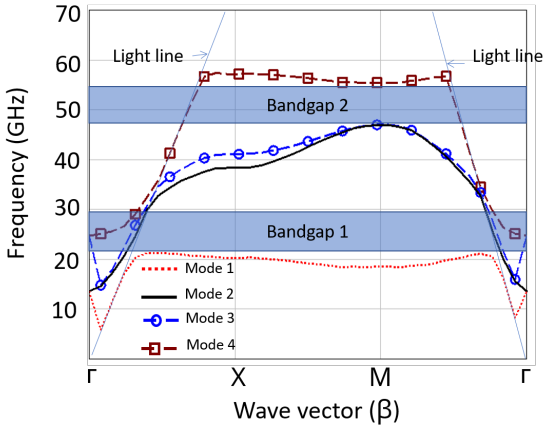

Fig. 4. Extracted bandgap diagram of mushroom structures

results, the EBG board has slightly less bandwidth than the Tx and Rx board without EBG. The bandwidth reduction effect due to EBG structures can be seen from the input impedance of the Tx antenna, as shown in Fig. 7. The slope of imaginary part of the Tx and Rx board with EBG structures increases in the regime of 26 GHz. The maximum realized gain of the antennas with and without EBG is reduced from 7.64 dBi to 7.6 dBi. The simulated maximum realized gain values with respect to the frequency of the Tx and Rx board with EBG structures are given in Fig. 8. The antennas have 7.6 dBi gain in the regime of 26 GHz, whereas the isolation of the antenna is increased from 22 dB to more than 50 dB over a bandwidth of 800 MHz in the regime of 26 GHz according to the simulation results. The 3D simulated gain pattern comparison is shown in Fig. 9. The pattern is slightly tilted due the EBG structures but, overall, the antenna radiation pattern is closely sustained.

The fabricated Tx and Rx board with EBG structures is shown in Fig. 10. The measured and simulated results of the Tx and Rx board with EBG structures are shown in Fig. 11. A close agreement is found between the simulated and measured results. However, there is a slight shift in the transmission coefficient due to the fabrication tolerance of sub-wavelength EBG metal patches and the via drill tolerance. The gain of the Tx and Rx antenna board with EBG is measured around 6 dBi with a known horn antenna in the E-plane.

IV. System Evaluation for Joint Communication and Sensing Application

Despite the recent increased interest in in-band full duplex systems for communications, these are still relatively

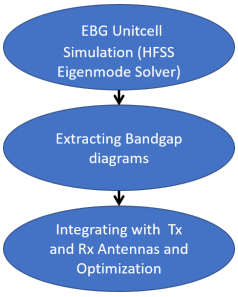

Fig. 5. Simulation design flow of the increasing the isolation between Tx and Rx antennas

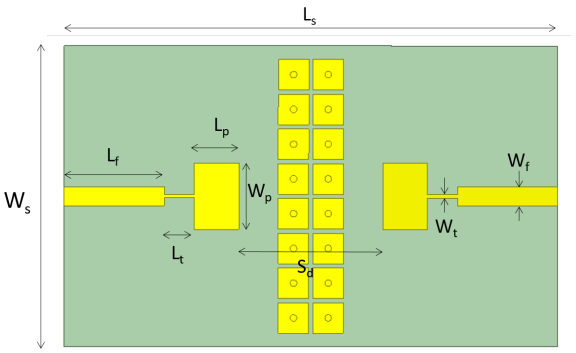

Fig. 6. Simulation model with highlighted dimensions of Tx and Rx antenna with EBG

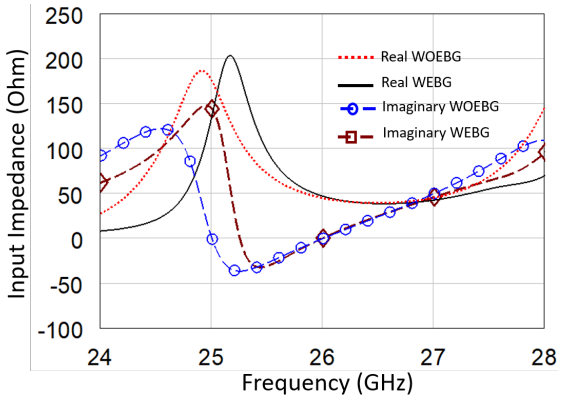

Fig. 7. Comparison of input impedance of the Tx antenna with EBG (WEBG) and without EBG (WOEBG)

TABLE I
Tx and Rx antenna board dimensions with and without EBG structures

Parameters	Without EBG (mm)	With EBG (mm)
L_s	26.875	29.61
W_s	18	18
L_p	2.675	2.68
W_p	3.977	3.977
L_f	6	6
W_f	1.136	1.136
L_t	1.88	1.8
W_t	0.3	0.2
U_{cx}	-	2.08
U_{cy}	-	2.08
g	-	0.125
D_{sc}	-	0.4
t	0.508	0.508

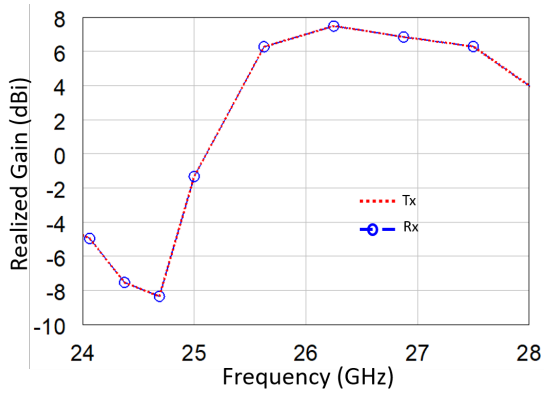

Fig. 8. Simulated maximum realized gain values with respect to different frequencies of the Tx and Rx board with EBG structures

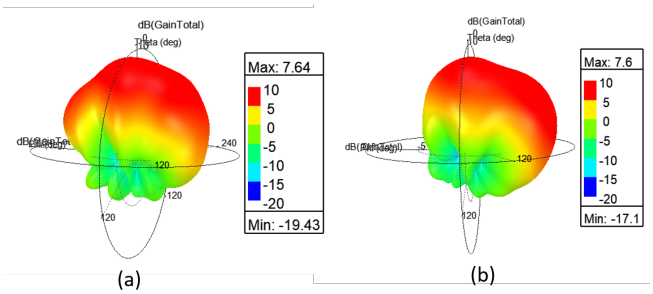

Fig. 9. 3D gain pattern of Tx and Rx antenna (a) without EBG (b) with EBG

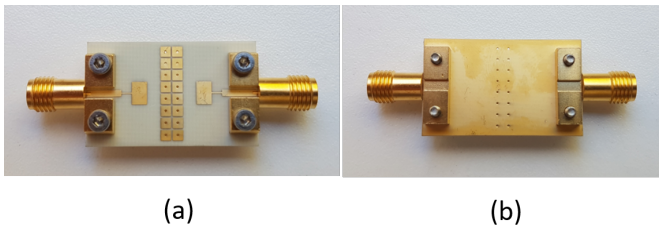

Fig. 10. Fabricated boards of Tx and Rx antenna with EBG structures (a) Top side (b) Bottom side

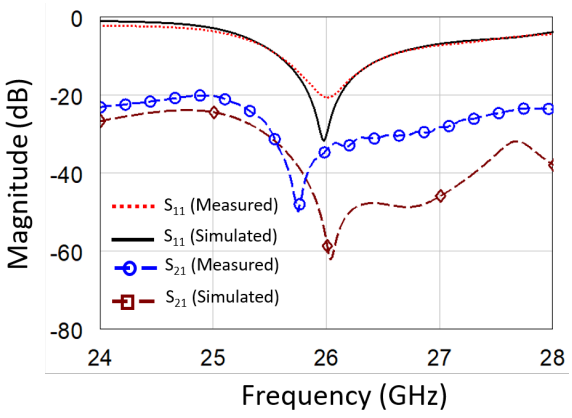

Fig. 11. Comparison of simulated and measured results of Tx and Rx antenna board with EBG

TABLE II
PERFORMANCE COMPARISON OF TX AND RX ANTENNA BOARD WITH AND WITHOUT EBG ACCORDING TO THE SIMULATION RESULTS

Parameters	Without EBG	With EBG
Bandwidth (MHz)	1090	977
Maximum Gain (dBi)	7.64	7.6
Isolation (dB)	22	62

expensive and have a high energy consumption [10], and, on account of that, wireless communications systems still rely on half-duplex techniques, like time-division duplexing (TDD). Therefore, the isolation between Tx and Rx is in general not necessarily a relevant issue for communications.

The situation is different for radar systems, which are likely to use pulses of long duration, like FMCW or orthogonal frequency-division multiplexing (OFDM), such that the self-interference from the transmitted signal and the received radar reflection overlap in time. In this case, the isolation between Tx and Rx becomes crucial, as the target echos may arrive with a very high attenuation and may be drowned by the self interference, which can have a power many orders of magnitude higher and, thus, saturate the receiver.

The question to be answered is how much isolation is required for a given JC&S scenario. It depends on lots of factors, like the waveform parameters, mixer and low-noise amplifier (LNA) saturation levels, and the expected path loss PL from the echo, which itself depends on the range R, wavelength λ_0, antenna gains G_tx and G_rx, and the radar cross section (RCS) σ, according to the radar range equation:

$$PL = \frac{G_{\text{tx}} G_{\text{rx}} \lambda_0^2 \sigma}{(4/pi)^3 R^4} \tag{1}$$

In order to evaluate the impact of different isolation levels, we have simulated radar detection for two different waveforms, namely FMCW and OFDM, using our Python open-source link-level simulator, Hermes [11]. At the receiver we consider an ideal automatic gain control (AGC), such that the dynamic range of the quantizer at the analog-to-digital converter (ADC) is exactly the same as in the received signal. This means, however, that the quantizer resolution may not be enough for the low-power echo.

The scenario for the simulations is listed in Table III, considering a single target.

TABLE III
SIMULATION SCENARIO PARAMETERS

Parameters	Value
range R	100 m
carrier frequency f_0	26 GHz
RCS σ	1 m^2
SNR	-10 dB
antenna gains G_tx and G_rx	5 dB
ADC resolution	8 bits

We first performed some simulations considering an FMCW (or chirp) radar, using stretch processing, i.e., we mix the

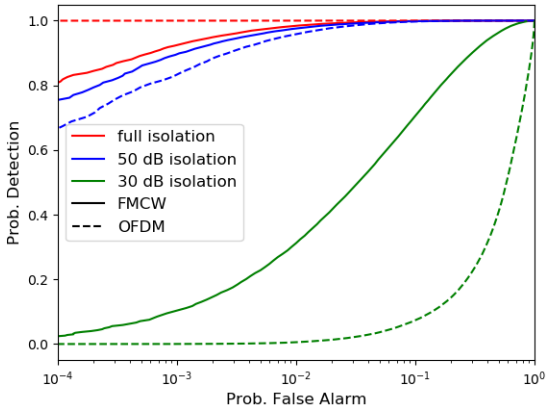

Fig. 12. ROC with SNR=-10 dB

received signal with the generated waveform to obtain beat frequencies proportional to the target ranges. Here, only in-phase mixing is considered. The self-interference component will generate a DC component, which is filtered out by a high-pass filter with cut-off frequency f_{min}. Considering a chirp bandwidth B, the signal is then filtered with a low-pass filter with cut-off frequency $f_{\text{max}} < B$, such that it can be sampled with a lower sampling frequency. The frequencies f_{min} and f_{max} correspond to the range window of the radar, i.e., considering $R_{\text{min}} = cf_{\text{min}}\tau/B$ and $R_{\text{max}} = cf_{\text{max}}\tau/B$, with τ the chirp duration, we can only observe the range R in the window $R_{\text{min}} < R < R_{\text{max}}$. After sampling, an FFT can be used to detect the beat frequencies, and, consequently, the ranges corresponding to the target echos.

We also simulated an OFDM radar, using the symbol-based approach described in [12], with parameters being chosen such that similar pulse repetition intervals and bandwidths are observed for both FMCW and OFDM. The waveform parameters are listed in Table IV, and the receiver operation characteristics (ROC) curves for an signal-to-noise ratio (SNR) of -10 dB with different isolation levels are depicted in Fig. 12. Note that low SNRs can be achieved from the processing gain $B\tau$ for FMCW and N_c for OFDM [12].

TABLE IV
WAVEFORM PARAMETERS

Waveform	Parameters	Value
FMCW	bandwidth B	100 MHz
	chirp duration τ	4 μ s
	maximum range R_{max}	200 m
OFDM	subcarrier spacing Δf	312.5 kHz
	guard interval T_G	800 ns
	FFT size N_{FFT}	512
	number of subcarriers N_c	384

We observe that the radar performance is severely degraded by the self interference, especially for OFDM radar, which has a high peak-to-average power ratio (PAPR) and cannot make use of the DC blocking approach used in stretch processing with FMCW. Depending on the system parameters, a 50 dB isolation can provide however a performance close to the one with full isolation, i.e., without self interference, as it can be seen in the FMCW results. A higher isolation may require a higher ADC resolution or further analog and digital processing, which are outside the scope of this paper.

V. CONCLUSIONS

In this paper, we have proposed a novel approach to address the challenge of maintaining high isolation between the transmitter and receiver antennas. Meta-surfaces as passive elements with high impedance and low power characteristics are used to suppress the surface waves and to increase the isolation between transmitter and receiver from 22 dB to 50 dB, experimentally. Furthermore, these results are used to measure system performance and demonstrate the improvement of radar system performance, increasing the isolation between the transmitter and receiver for the future joint communication and sensing applications. As a future work, the target will be to explore more meta-surfaces with similar isolation values and constant attenuation characteristics over a wider frequency band.

ACKNOWLEDGEMENT

This work is financed by the Saxon State government out of the State budget approved by the Saxon State Parliament. The authors would like to acknowledge the contribution of Tim Hentschel to this work.

REFERENCES

[1] C. de Lima *et al.*, "Convergent communication, sensing and localization in 6G systems: An overview of technologies, opportunities and challenges," *IEEE Access*, vol. 9, 2021.
[2] F. Liu *et al.*, "Joint radar and communication design: Applications, state-of-the-art, and the road ahead," *IEEE Transactions on Communications*, vol. 68, no. 6, pp. 3834–3862, 2020.
[3] P. Hindle, "Comprehensive survey of 77, 79 GHz automotive radar companies – sensors and ICs," *Microwave Journal*, March 2020.
[4] M. Biedka, Y. E. Wang, Q. M. Xu, and Y. Li, "Full-duplex rf front ends : From antennas and circulators to leakage cancellation," *IEEE Microwave Magazine*, vol. 20, no. 2, pp. 44–55, 2019.
[5] D. M. Pozar, "Input impedance and mutual coupling of rectangular microstrip antennas," *IEEE Transactions on Antennas and Propagation*, vol. 30, no. 6, pp. 1191–1196, 1982.
[6] C. A. Balanis, *Antenna Theory: Analysis and Design*. 3rd ed. Hoboken, USA: Wiley, 2005.
[7] G. M. Brooker, "Understanding millimetre wave FMCW radars," in *1st International Conference on Sensing Technology, IEEE, New Zealand, 2005*, pp. 152–157.
[8] F. Yang and Y. Rahmat-Samii, "Microstrip antennas integrated with electromagnetic band-gap (ebg) structures: a low mutual coupling design for array applications," *IEEE Transactions on Antennas and Propagation*, vol. 51, no. 10, pp. 2936–2946, 2003.
[9] L. Peng, C.-l. Ruan, and J. Xiong, "Compact ebg for multi-band applications," *IEEE Transactions on Antennas and Propagation*, vol. 60, no. 9, pp. 4440–4444, 2012.
[10] V. Singh, A. Gadre, and S. Kumar, "Full duplex radios: Are we there yet?" in *ACM Workshop on Hot Topics in Networks (HotNets)*, Nov. 2020.
[11] "HEterogeneous Radio MobilE Simulator in Python (HermesPy) - https://github.com/barkhausen-institut/hermespy."
[12] C. Sturm and W. Wiesbeck, "Waveform design and signal processing aspects for fusion of wireless communications and radar sensing," *Proceedings of the IEEE*, vol. 99, no. 7, pp. 1236–1259, 2011.